This article has been accepted for publication in IEEE Transactions on Medical Robotics and Bionics. This is the author's version which has not been fully edited and content may change prior to final publication. Citation information: DOI 10.1109/TMRB.2026.3753078

Real-Time Leak Detection in a Soft Everting Robotic Colonoscope

Korn Borvorntanajanya, *Graduate Student Member, IEEE*, Jialei Shi, Fung Flora Leung, Philip Wai Yan Chiu, Enrico Franco, and Ferdinando Rodriguez y Baena, *Member, IEEE*

***Abstract*— Leakage is a critical safety concern in pneumatically actuated soft everting colonoscopes, where ruptures or seal failures can cause unintended strain transmitted to the colon wall. Detecting leakage during operation is challenging because inlet-flow naturally varies due to volume expansion during growth and pressure regulation. As a result, simple thresholding filters could generate false detections and often miss true leaks. This paper introduces an extended Kalman Filter (EKF)-based residual leak detection approach that decomposes the measured inlet flow into geometric, regulatory, and leakage components, allowing required actuation-related flow to be separated from excess flow resulting from leakage. Experimental validation demonstrates that the proposed approach reduces false-positive leak alarms by over 98%, maintains sub-second detection delay, and reduces peak environmental pressure in the collapsed phantom by approximately 59% under the tested conditions. Under the tested phantom conditions, EKF-based detection reduced the peak measured environmental pressure to $(0.049 \pm 0.01\ \mathrm{bar})$. These results indicate that the proposed approach provides fast and reliable leak detection while reducing pressure exposure during leakage events in soft everting devices for gastrointestinal interventions.**

***Index Terms*—Soft Growing Robot, State Estimation, Leak Detection, Colonoscopy.**

I. Introduction

CONVENTIONAL colonoscopy is often uncomfortable because the scope is advanced by pushing. As the scope is pushed through a long, tortuous colon, it can stretch the colon and generate stress on the bowel wall, which patients perceive as pain [1]. Soft everting colonoscopes aim to reduce patient's discomfort [2] by using pneumatic pressure to evert a thin-walled sleeve from the tip, so the device advances with minimal shear on the bowel [3]. Specifically, internal pressure turns a thin-walled tube inside out at the tip while a spool at the base unreels stored material, continuously creating new outer wall from the inner layer [4]. As such, soft everting robots can navigate complex, confined colon environments without relying on friction against surrounding tissue.

Although eversion-based robots have shown potential to improve outcomes in minimally invasive procedures [5]–[7], leakage remains a safety concern in medical settings. Accidental mechanical damage or excessive internal pressure may cause the thin-walled sleeve to rupture during eversion. Air may also escape if a seal fails. If air enters the colon lumen, continued air delivery may distend the bowel and increase pressure on its wall. Excessive insufflation can cause colonic injury or perforation [8]. In human cadaver experiments, colonic rupture occurred at mean intraluminal pressures of $0.11\ \mathrm{bar}$ in the cecum and $0.23\ \mathrm{bar}$ in the sigmoid colon [9]. A leak can also reduce the pressure supporting the robot, potentially concentrating contact forces where the device bends (Fig. 1). These risks motivate prompt detection and interruption of the air supply.

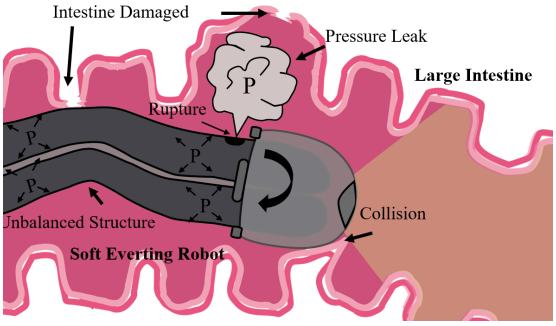

Fig. 1. Potential hazards of sleeve rupture: escaping air may increase bowel pressure when gas escape is restricted, while loss of robot pressure may alter contact with the bowel wall.

In practice, leakage presents as a combination of pressure drop and elevated inlet flow. However, both signals also vary during normal operation. As the robot grows, its internal volume expands and the pressure regulator supplies additional air. Changes in commanded pressure similarly produce transient flow surges. These behaviours make reliable leakage detection challenging, because simple pressure or flow thresholds can confuse normal growth-induced fluidic changes with leakage.

To address this challenge, this work proposes an extended Kalman filter (EKF)-based residual leak detector for a soft everting colonoscope. The detector algorithm runs on the robot's control computer and uses commanded spool speed and growth pressure, together with measured pressure and inlet flow, to predict the inlet flow expected during normal operation. A suspected leak is identified when measured flow exceeds this prediction by a specified threshold for a specified duration, triggering automatic pneumatic supply cutoff.

The main contribution is the formulation and experimental evaluation of a leak detector that accounts for both growth-induced volume change and pressure-regulation dynamics during commanded growth.

II. Related Works

Leakage is a critical failure mode in fluidically driven soft robots because it directly affects pressure regulation, motion

Received 13 December 2025; revised 18 June 2026 and 1 October 2026 ;accepted 5 November 2026. Date of publication ..... This article was recommended for publication by Associate Editor L. Manfredi and Editor F. Ficuciello upon evaluation of the reviewers' comments. This work has been supported by the Engineering and Physical Sciences Research Council, Grant EP/X033546/1, Imperial UKRI IAA, Grant EP/X52556X/1 and partially by InnoHK, Multiscale Robotics Centre, The Chinese University of Hong Kong. (*Corresponding author: Ferdinando Rodriguez y Baena*)

K. Borvorntanajanya, J. Shi, E. Franco, and F. Rodriguez y Baena are with The Hamlyn Centre for Robotic Surgery, Imperial College London, London, United Kingdom (email: f.rodriguez@imperial.ac.uk).

F. F. Leung and P. W. Y. Chiu are with the Multiscale Medical Robotics Center, The Chinese University of Hong Kong, Hong Kong SAR, China (email: philipchiu@cuhk.edu.hk).

Digital Object Identifier ....

Authorized licensed use limited to: Imperial College London. Downloaded on November 21,2026 at 20:48:29 UTC from IEEE Xplore. Restrictions apply.
© 2026 IEEE. All rights reserved, including rights for text and data mining and training of artificial intelligence and similar technologies. Personal use is permitted, but republication/redistribution requires IEEE permission. See https://www.ieee.org/publications/rights/index.html for more information.

This article has been accepted for publication in IEEE Transactions on Medical Robotics and Bionics. This is the author's version which has not been fully edited and content may change prior to final publication. Citation information: DOI 10.1109/TMRB.2026.3753078

repeatability, and system reliability [10]. Various damage-sensing methods have been explored in soft robotics, including resistive, optical, pneumatic, vision-based, and robot-performance-based approaches [11]. While these methods can provide useful information for damage detection, many require additional sensors, increasing system integration complexity.

In contrast, pressure and flow measurements are intrinsic to many pneumatic soft robotic systems and can therefore be used for leakage detection without adding extra sensors to the system. Existing leakage-detection approaches in pneumatic and soft robotic systems often rely on pressure-based indicators, such as abnormal pressure decay, burst-pressure events, or threshold-based changes in chamber pressure [12]–[14]. However, pressure alone can be ambiguous in soft robots because intentional actuation, environmental contact, and body deformation can all change the measured pressure without a leak [15], [16]. To reduce this ambiguity, several studies have incorporated flow-related information together with pressure sensing. Combining flow with pressure measurements provides information about actuator volume change [6], [17]. In a soft everting robot, commanded growth increases the internal volume and requires inlet flow even without a sleeve leak. Flow rates of up to 12 SLM have been reported during such operation at an internal actuation pressure of 0.25 bar [4]. Because both growth and leakage require inlet flow, and the regulator may maintain the measured base pressure during a leak, neither flow nor pressure alone reliably distinguishes leakage from the flow required for eversion.

As summarized in Table I, existing pressure-drop or pressure–flow thresholding methods have mainly been demonstrated in systems with relatively small volume changes. This motivates a residual-based detector that compares the measured pressure–flow response with the expected response under normal growth.

III. System Overview and Sensing

The design of the soft growing colonoscope is described in [6]. As shown in Fig. 2, the robot is actuated by two low-level commands: the spool command ω_k and the growth-pressure command P_k^{grow}. The command ω_k sets the angular speed of the material spool and controls the release of the stored everting sleeve; it is also used to compute the growth velocity v_k. The command P_k^{grow} defines the target internal pressure of the eversion structure.

TABLE I: Comparison of leakage and fault detection methods. Delay is the time from fault onset to detection; performance is the percentage of faults correctly detected.

Method	Ref.	System	Volume Change	Additional Sensor	Delay	Performance
Pressure drop	[12]	Pneumatic Pouches	Small	✗	1.6 s	N/R
Pressure threshold	[13]	Pneumatic Finger	Small	✓	0.021 s	N/R
Pressure threshold	[14]	Pneumatic logic system	Small	✓	6 s	100%
Pressure threshold	[16]	Soft pressure sensor	Small	✗	N/R	93%
Flow threshold	[6]	Pneumatic manipulator	Small	✗	0.15 s	N/R
Proposed EKF	*	Soft growing robot	Large	✗	0.38 s	97.5%

* this work, N/R: not reported.

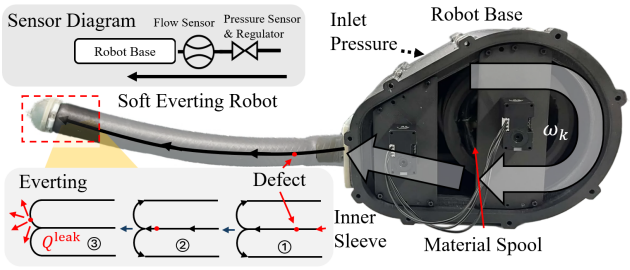

Fig. 2. Soft everting robotic colonoscope and sensing layout. The lower schematic illustrates sleeve eversion at the distal region marked by the red box. Stages 1–3, read from right to left, show a defect travelling along the inner sleeve and becoming exposed to the environment at the eversion tip, producing leak flow. Black arrows along the sleeve indicate material motion, while red arrows radiating from the exposed defect indicate escaping air.

At each time step k, the controller sends ω_k and P_k^{grow} to the low-level actuation system. The pressure regulator drives the measured internal pressure P_k^{mea} toward P_k^{grow} by supplying or venting air at the robot inlet. As the sleeve everts and the internal volume changes, this pressure-regulation process generates an inlet flow $Q_k^{\mathrm{mea,in}}$. Therefore, $Q_k^{\mathrm{mea,in}}$ is not directly commanded by the controller, but is measured as the flow required to track the commanded growth pressure during eversion. During operation, the available measurements are the internal pressure P_k^{mea} from the base-mounted pressure sensor, the inlet flow $Q_k^{\mathrm{mea,in}}$ from the inline flow sensor, and the spool angular velocity ω_k from the servo encoder.

IV. EKF-Based Residual Leak Detector

This section presents the no-leak inlet-flow model, the EKF state prediction and measurement update, and the residual-based detection rule. The flow residual is computed before each measurement update by comparing the measured inlet flow with the EKF prediction. The EKF provides a model-based prediction that can be updated in real time without requiring a labelled dataset for model calibration [18].

A. Expected No-Leak Inlet Flow

At the k-th time step, the inlet flow expected during normal operation is modelled as

$$Q_k^{\mathrm{exp}} = Q_k^{\mathrm{geom}} + Q_k^{\mathrm{press}} + Q_{\mathrm{leak}}^{\mathrm{base}}, \tag{1}$$

where Q_k^{geom} is the flow required to fill the newly deployed volume, Q_k^{press} is the additional flow caused by pressure regulation, and $Q_{\mathrm{leak}}^{\mathrm{base}}$ is the constant baseline leakage measured from calibration.

The geometric growth flow is written as

$$Q_k^{\mathrm{geom}} = A\kappa_V\omega_k, \tag{2}$$

where A is the cross-sectional area of the everting cavity, ω_k is the spool speed, and κ_V is a calibrated conversion factor between spool speed and tip growth speed. The cavity volume is updated as

$$V_k = V_{k-1} + Q_{k-1}^{\mathrm{geom}}\Delta t. \tag{3}$$

The pressure-regulation flow is modelled as

$$Q_k^{\mathrm{press}} = \alpha_p\left(P_k^{\mathrm{grow}} - P_k^{\mathrm{mea}}\right) + \alpha_d\left(P_k^{\mathrm{grow}} - P_{k-1}^{\mathrm{grow}}\right), \tag{4}$$

where α_p represents the influence of steady pressure error on inflow and α_d models the flow transient that occurs when the

Authorized licensed use limited to: Imperial College London. Downloaded on November 21,2026 at 20:48:29 UTC from IEEE Xplore. Restrictions apply.
© 2026 IEEE. All rights reserved, including rights for text and data mining and training of artificial intelligence and similar technologies. Personal use is permitted, but republication/redistribution requires IEEE permission. See https://www.ieee.org/publications/rights/index.html for more information.

This article has been accepted for publication in IEEE Transactions on Medical Robotics and Bionics. This is the author's version which has not been fully edited and content may change prior to final publication. Citation information: DOI 10.1109/TMRB.2026.3753078

commanded pressure is stepped. Both α_p and α_d are constant gains with units of $\mathrm{SLM/bar}$, identified from calibration experiments that map pressure changes to corresponding inflow.

B. EKF State and Process Model

The EKF state is defined as $\mathbf{x}_k = \left[P_k, Q_k^{\mathrm{in}}\right]^\top$, where P_k is the internal pressure and Q_k^{in} is the predicted inlet flow required under no-leak operation. The pressure prediction is obtained from an isothermal gas balance under the no-leak assumption:

$$\hat{P}_{k+1|k} = \hat{P}_{k|k} + \frac{C_Q\left(Q_k^{\mathrm{exp}} - Q_{\mathrm{leak}}^{\mathrm{base}}\right) - \hat{P}_{k|k} Q_k^{\mathrm{geom}}}{V_k}\Delta t. \tag{5}$$

where C_Q is a constant conversion factor that converts inlet flow in SLM into the pressure–volume rate. The no-leak inlet flow state is updated toward the expected inlet flow as

$$\hat{Q}_{k+1|k}^{\mathrm{in}} = \hat{Q}_{k|k}^{\mathrm{in}} + \beta\left(Q_k^{\mathrm{exp}} - \hat{Q}_{k|k}^{\mathrm{in}}\right), \tag{6}$$

where $\beta \in (0, 1]$ is a smoothing factor.

The EKF prediction step is therefore written as

$$\begin{aligned} \hat{\mathbf{x}}_{k+1|k} &= f\left(\hat{\mathbf{x}}_{k|k}, \mathbf{u}_k\right), \\ \Sigma_{k+1|k} &= A_k \Sigma_{k|k} A_k^\top + q, \end{aligned} \tag{7}$$

where $\mathbf{u}_k = [\omega_k,\ P_k^{\mathrm{grow}}]^\top$ is the known input, q is the process-noise covariance, and $A_k = \left.\frac{\partial f}{\partial \mathbf{x}}\right|_{\hat{\mathbf{x}}_{k|k}}$ is the process-model Jacobian.

C. EKF Measurement Update

The measurement vector is $\mathbf{z}_k = \left[P_k^{\mathrm{mea}}, Q_k^{\mathrm{mea,in}}\right]^\top$. The measurement model is

$$\mathbf{z}_k = h(\mathbf{x}_k) + \mathbf{v}_k, \qquad h(\mathbf{x}_k) = \begin{bmatrix} P_k \\ Q_k^{\mathrm{in}} \end{bmatrix}, \tag{8}$$

where $\mathbf{v}_k$ is the measurement noise. The measurement Jacobian is therefore $H_k = \begin{bmatrix} 1 & 0 \\ 0 & 1 \end{bmatrix}$.

The EKF correction is

$$\begin{aligned} \mathbf{y}_{k+1} &= \mathbf{z}_{k+1} - h\left(\hat{\mathbf{x}}_{k+1|k}\right), \\ S_{k+1} &= H_{k+1}\Sigma_{k+1|k}H_{k+1}^\top + R, \\ K_{k+1} &= \Sigma_{k+1|k}H_{k+1}^\top S_{k+1}^{-1}, \\ \hat{\mathbf{x}}_{k+1|k+1} &= \hat{\mathbf{x}}_{k+1|k} + K_{k+1}\mathbf{y}_{k+1}, \\ \Sigma_{k+1|k+1} &= \left(I - K_{k+1}H_{k+1}\right)\Sigma_{k+1|k}. \end{aligned} \tag{9}$$

D. Residual-Based Leak Decision

The leak decision is made using the EKF prior prediction before measurement correction. The flow residual is defined as

$$r_{k+1} = Q_{k+1}^{\mathrm{mea,in}} - \hat{Q}_{k+1|k}^{\mathrm{in}}. \tag{10}$$

The residual r_{k+1} represents the surplus inlet flow that cannot be explained by geometric growth, pressure regulation, or the calibrated baseline leak. Under normal no-leak operation, this residual remains close to zero except for sensor noise and short regulator transients. When a rupture occurs, additional inlet flow is required to compensate for escaping air, resulting in a persistent positive residual.

Algorithm 1 EKF-based residual leak detector

Require: Initial state $\hat{\mathbf{x}}_{0|0}$, covariance $\Sigma_{0|0}$, initial volume V_0
for each sampling step k **do**
  Read P_k^{mea}, $Q_k^{\mathrm{mea,in}}$, ω_k, and P_k^{grow}
  Compute Q_k^{geom}, Q_k^{press}, and Q_k^{exp} using (2), (4), and (1)
  Update the cavity volume V_k using (3)
  Perform the EKF prediction using (5), (6), and (7)
  Compute the flow residual r_{k+1} using (10)
  Perform the EKF measurement correction using (9)
  Apply the residual threshold, dwell-time rule, and leak latching
end for

A binary leak flag ℓ_k is introduced only at the detector level and is not part of the EKF state. The flag is updated using a threshold and dwell-time rule:

$$\ell_{k+1} = \begin{cases} 1, & r_{k+1} > r_{\mathrm{th}} \text{ for at least } N_{\mathrm{dwell}} \text{ consecutive samples}, \\ \ell_k, & \text{otherwise}, \end{cases} \tag{11}$$

where r_{th} is the residual threshold and N_{dwell} is the dwell-time requirement. Once $\ell_k = 1$, the flag remains active because leakage may continue even when the residual falls below the threshold. The overall EKF-based residual computation and leak-detection procedure are summarised in Algorithm 1.

V. Experimental Validation

Experiments were carried out on the everting robotic colonoscope described in [6], equipped with a pressure regulator (SMC ITV2010, G3/8) and an inline flow sensor (Sensirion SFM4300). The material spool was driven by a DYNAMIXEL XL330 servo motor via USB, with velocity commands sent from MATLAB R2024a. The EKF ran at 50 Hz, with each iteration requiring approximately 14 ms in MATLAB. The pressure and flow sensors were sampled at 50 Hz, and the regulator command was updated at 20 Hz. The regulator has a nominal no-load pressure response of approximately 0.1 s.

A. Experimental Protocols

Experiments were conducted under the three test conditions summarized in Table II. Condition I (free space) provided leak-free data for model calibration and allowed leak-related pressure and flow changes to be evaluated without wall contact. Condition II used an S-shaped phantom to assess leak detection during navigation through successive bends and wall contact. Condition III used a closed-ended collapsed phantom to assess pressure accumulation after leakage and the effect of automatic pneumatic supply cutoff. The different phantom configurations therefore evaluated detection during curved navigation and pressure mitigation in a deformable, confined environment, respectively.

Repeatable leaks were created by puncturing the sleeve at specified distances from the initial eversion point, with the punctures opening to the environment during growth. The ground-truth leak onset time t_0 was obtained by offline annotation, using synchronized video to identify when the defect opened and aligning this time with the inlet-flow trace.

Throughout all trials, growth was commanded using a fixed active spool speed of $\omega_k = 7.2$ rpm, corresponding to $v_k \approx 0.02$ m/s. The commanded growth pressure P_k^{grow} was manually varied during navigation within 0.0–0.16 bar, resulting in arbitrary pressure-step magnitudes within this

Authorized licensed use limited to: Imperial College London. Downloaded on November 21,2026 at 20:48:29 UTC from IEEE Xplore. Restrictions apply.
© 2026 IEEE. All rights reserved, including rights for text and data mining and training of artificial intelligence and similar technologies. Personal use is permitted, but republication/redistribution requires IEEE permission. See https://www.ieee.org/publications/rights/index.html for more information.

This article has been accepted for publication in IEEE Transactions on Medical Robotics and Bionics. This is the author's version which has not been fully edited and content may change prior to final publication. Citation information: DOI 10.1109/TMRB.2026.3753078

TABLE II: Experimental test conditions, with 20 trials conducted under each condition. r denotes the measured radius of the leak.

Condition	Environment	Leak location	Leak severity
I	Free space	54 cm	Moderate ($r \leq 1$ mm)
II	S-shaped phantom	130 cm	Small ($r \leq 0.5$ mm)
III	Collapsed phantom	80 cm	Moderate ($r \leq 1$ mm)

tested range. The EKF was initialised only after the pressure reached 0.05 bar so that the initial transient did not bias the estimate. Further details of these experiments are provided in the Supplementary Video.

1) Experiment 1 No-Leak Model Calibration: This experiment calibrated the no-leak inlet-flow model in (1) and evaluated its calibration accuracy. Calibration used the leak-free portions of the Condition I trials, before the robot reached $50\,\mathrm{cm}$ of eversion. These data captured normal flow variations associated with growth and pressure regulation, including baseline leakage from the pneumatic supply and base connection. The baseline leakage $Q_{\mathrm{leak}}^{\mathrm{base}}$ was estimated from steady pressurized intervals without growth, and Q^{geom} was computed from the commanded growth velocity and tube cross-sectional area. The pressure-regulation gains were fitted to the calibration data by minimizing the sum of squared flow residuals in (10).

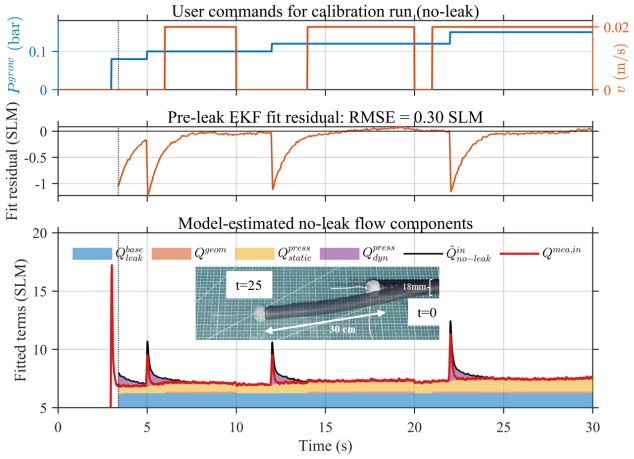

Fig. 3. Representative no-leak calibration trial for identifying the inlet-flow model parameters. The top and middle panels show the commanded inputs and EKF fit residual, respectively. The bottom panel compares the measured inlet flow with the model-estimated no-leak flow.

2) Experiment 2 Leak Detection During Commanded Growth: This experiment evaluated leak detection during commanded growth, quantifying false positives, false negatives, and detection delay under varying actuation commands. A total of 40 trials were conducted under test conditions I and II in Table II. Three detection methods were evaluated.

The first baseline applied a direct inlet-flow threshold, following [6]. A leak was declared when $Q_k^{\mathrm{mea,in}} \geq Q_{\mathrm{th}}$, where $Q_{\mathrm{th}} = 11\,\mathrm{SLM}$ was selected empirically from separate leak-free and induced-leak calibration trials.

The second baseline used pressure-drop thresholding to assess leak detection using the base-mounted pressure sensor alone. The pressure-drop feature was computed as $\Delta P_k = P_{k-N_w}^{\mathrm{mea}} - P_k^{\mathrm{mea}}$, where N_w corresponds to a $0.5\,\mathrm{s}$ window. A leak was declared when $\Delta P_k \geq \Delta P^{\mathrm{th}}$, with $\Delta P^{\mathrm{th}} = 0.05\,\mathrm{bar}$.

The third method used the proposed EKF-based residual detector. The no-leak model parameters identified in Experiment 1 were kept fixed. Detector performance was evaluated by sweeping the residual threshold r_{th} from 1 to $4\,\mathrm{SLM}$ and the dwell time T_{dwell} from 0.1 to $0.4\,\mathrm{s}$.

Performance was evaluated using false-positive and false-negative counts and detection delay. A false positive was recorded when an alarm occurred during the leak-free portion of a trial. A false negative was recorded when no alarm occurred between leak onset and the end of the observation period. For detected leaks, the detection delay was defined as $t_{\mathrm{detect}} = t_{\mathrm{alarm}} - t_0$, where t_0 denotes the ground-truth leak onset time and t_{alarm} denotes the first alarm. The baselines reset below threshold and could trigger repeatedly, whereas the EKF alarm remained latched after its first detection.

3) Experiment 3 Navigation in a Collapsed Phantom: This experiment evaluated whether EKF-based leak detection with automatic pneumatic supply cutoff reduced environmental pressure following a leak during navigation in a collapsed soft phantom. The experiment used test condition III. The phantom was $1.2\,\mathrm{m}$ long, made of nylon fabric, and had an inner diameter of $40\,\mathrm{mm}$. The phantom was loosely secured at four points, allowing it to deform as the robot advanced. An external pressure sensor (4525DO, TE Connectivity) was connected to the phantom to measure its internal environmental pressure, $P_{\mathrm{env}}(t)$, as illustrated in Fig. 5(a3,b3).

Two operating modes were compared, with 10 trials per mode under varying control inputs. In the detection-disabled mode, the EKF detector was inactive and the regulator continued supplying pressure after leak onset. The operator manually stopped the system after the environmental pressure reached a steady state. In the detection-enabled mode, the EKF-based residual detector operated online, and the controller automatically shut off the pneumatic supply when a leak was detected ($\ell_k = 1$). For each trial, environmental pressure was evaluated from the annotated leak onset t_0 to the end of

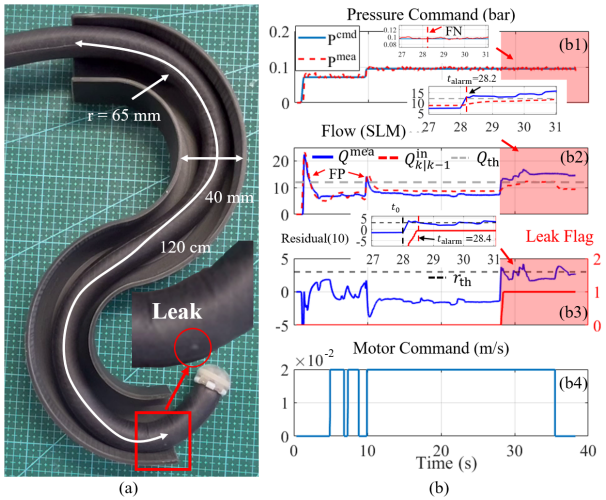

Fig. 4. Representative leak detection trial. (a) Pre-damaged sleeve segment showing the induced leak location. (b) Commanded pressure (b1), measured inlet flow $Q_k^{\mathrm{mea,in}}$, predicted no-leak flow $\hat{Q}_{k|k-1}^{\mathrm{in}}$, and the thresholding filter Q_{th} (b2). The flow residual (10) rises after rupture, crosses the threshold r_{th}, and triggers the leak flag $\ell_k = 1$. Insets highlight the moment the residual surpasses threshold during growth (b3), and motor command (b4).

Authorized licensed use limited to: Imperial College London. Downloaded on November 21,2026 at 20:48:29 UTC from IEEE Xplore. Restrictions apply.
© 2026 IEEE. All rights reserved, including rights for text and data mining and training of artificial intelligence and similar technologies. Personal use is permitted, but republication/redistribution requires IEEE permission. See https://www.ieee.org/publications/rights/index.html for more information.

This article has been accepted for publication in IEEE Transactions on Medical Robotics and Bionics. This is the author's version which has not been fully edited and content may change prior to final publication. Citation information: DOI 10.1109/TMRB.2026.3753078

the analysed recording, t_{end}. Peak and mean environmental pressure were calculated as $P_{\max} = \max_{t_0 \le t \le t_{\text{end}}} P_{\text{env}}(t)$, and $\bar{P}_{\text{env}} = \frac{1}{t_{\text{end}} - t_0} \int_{t_0}^{t_{\text{end}}} P_{\text{env}}(t)\,\mathrm{d}t$.

B. Results

1) Experiment 1 No-Leak Model Calibration: After calibration, the no-leak model parameters were fixed and used unchanged in the subsequent leak-detection experiments. The calibrated no-leak model achieved a mean residual RMSE of $0.30\,\text{SLM}$ over the no-leak calibration trials. The calibrated parameters are summarized in Table III, and a representative no-leak fit is shown in Fig. 3.

TABLE III: Model parameters and calibration constants

Symbol	Description	Value
A	Cross sectional area of the everting tube	2.54×10^{-4} m^2
α_p	Pressure-error regulator gain	10 SLM/bar
α_d	Pressure-transition regulator gain	80 SLM/bar
$Q_{\text{leak}}^{\text{base}}$	Static base leakage	6.2 SLM
β	Flow smoothing gain	0.4

2) Experiment 2 Leak Detection During Commanded Growth: Figure 6 shows leak detection performance across the residual-threshold and dwell-time sweep. Increasing r_{th} or T_{dwell} generally reduced alarms before the ground-truth leak onset t_0, but higher thresholds or longer dwell times also resulted in more missed leaks. The setting $r_{\text{th}} = 3\,\text{SLM}$ and $T_{\text{dwell}} = 0.3\,\text{s}$ detected 39 of 40 leaks, with one early false alarm. This setting was selected for the subsequent comparison with the inlet-flow and pressure-drop baselines.

Figure 4(b) illustrates the responses of the three detection methods during a representative commanded-growth trial with a single induced leak. The measured inlet flow $Q_k^{\text{mea,in}}$ exhibited sharp transient peaks following changes in the pressure or motor command, as shown in Fig. 4(b1), (b2), and (b4). These command-induced surges crossed the direct inlet-flow threshold, producing several false alarms before leak onset. The pressure-drop baseline was sensitive to intentional reductions in the commanded growth pressure. These reductions caused the measured base pressure to drop even when no leak was present, resulting in false-positive detections.

The EKF-based detector accounted for command-induced flow variations through its prediction of the no-leak inlet flow, $\hat{Q}_{k|k-1}^{\text{in}}$, including the contributions of geometric filling and pressure regulation. The residual in Fig. 4(b3) therefore remained close to zero during normal growth and increased after leak onset. The EKF alarm occurred at $t_{\text{alarm}} = 28.43\,\text{s}$, corresponding to a detection delay of approximately $0.42\,\text{s}$.

Table IV summarizes performance across the 40 trials. Pressure-drop thresholding detected no true leaks. The single EKF false positive latched the alarm before leak onset, preventing the subsequent leak from being registered as a new event and resulting in one false negative (see Supplementary Materials).

3) Experiment 3: Navigation in a Collapsed Phantom: Figure 5 compares representative environmental pressure profiles with detection disabled and enabled. With detection disabled, pressure increased after leak onset and remained elevated until the operator manually stopped the system. With detection enabled, the EKF-based detector triggered automatic supply cutoff, limiting the pressure rise inside the phantom.

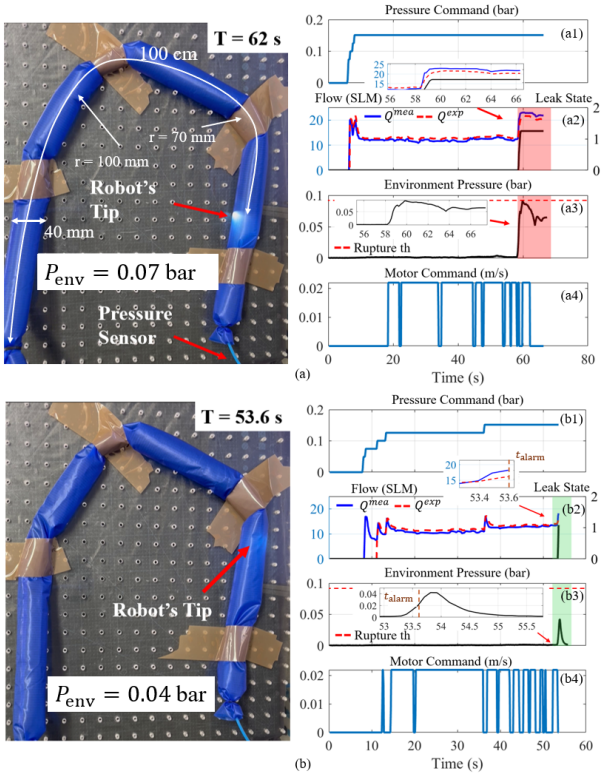

Fig. 5. EKF-based leak detection during navigation in a collapsed soft phantom. (**a**) Detection disabled: after leak onset, the regulator continues supplying pressure until the operator manually stops the system. (**b**) Detection enabled: the EKF residual triggers an automatic pressure cutoff shortly after leak onset, reducing the measured environmental pressure P_{env}.

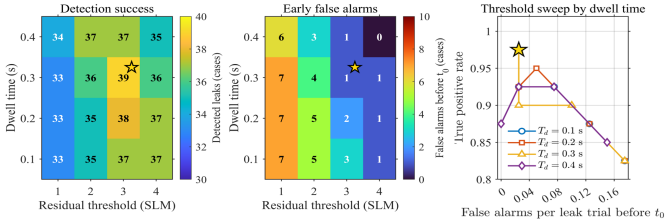

Fig. 6. Parameter sweep for the EKF-based residual detector in Experiment 2. Detection success, early false alarms before t_0, and the true-positive/false-alarm trade-off are shown for different residual thresholds r_{th} and dwell times T_{dwell}. The yellow star marks the selected operating point, $r_{\text{th}} = 3$ SLM and $T_{\text{dwell}} = 0.3$ s, which detected $39/40$ leaks with one early false alarm.

Across the 10 detection-enabled trials, all induced leaks were detected with no false positives or false negatives and a mean detection delay of $0.41 \pm 0.13\,\text{s}$ (Table V). Compared with detection disabled, enabling detection reduced peak environmental pressure from $0.12 \pm 0.05\,\text{bar}$ to $0.049 \pm 0.01\,\text{bar}$, a reduction of approximately 59%. Mean environmental pressure $\bar{P}_{\text{env}}$ decreased from $0.07 \pm 0.006\,\text{bar}$ to $0.008 \pm 0.003\,\text{bar}$, a reduction of approximately 89% ($p < 10^{-4}$).

VI. Discussion and Conclusion

This work introduced an EKF-based leak detector algorithm for a soft everting colonoscope. The algorithm uses inlet flow and pressure measurements, obtained from sensors located on the control unit, to identify leaks on the everting sleeve. This extends existing pressure- and flow-based approaches by

Authorized licensed use limited to: Imperial College London. Downloaded on November 21,2026 at 20:48:29 UTC from IEEE Xplore. Restrictions apply.
© 2026 IEEE. All rights reserved, including rights for text and data mining and training of artificial intelligence and similar technologies. Personal use is permitted, but republication/redistribution requires IEEE permission. See https://www.ieee.org/publications/rights/index.html for more information.

This article has been accepted for publication in IEEE Transactions on Medical Robotics and Bionics. This is the author's version which has not been fully edited and content may change prior to final publication. Citation information: DOI 10.1109/TMRB.2026.3753078

TABLE IV: Leak detection performance in Experiment 2 ($n = 40$). Delay is mean $\pm$ SD; p-values are vs. EKF.

Method	FP (count)	FN (count)	Detection Delay (s)	p-value
Thresholding	67	5/40	0.54 ± 0.41	0.32
Pressure drop	49	40/40	N/A	N/A
Proposed EKF	1	1/40	0.38 ± 0.08	–

FP: False Positives, FN: False Negatives

accounting for the changing flow demand associated with eversion. In Experiment 1, the calibrated model captured normal inlet-flow variations during simultaneous pressure regulation and growth, with a residual RMSE of 0.30 SLM. This provided a reference for assessing deviations from normal operation in the subsequent experiments.

In Experiment 2, the comparison with the threshold-based methods highlights the benefit of the proposed detector algorithm. Direct inlet-flow thresholding [6] generated false positives due to command-induced flow surges. Pressure-drop thresholding [14] generated false positives during intentional pressure reductions and missed leaks when the regulator maintained the baseline pressure. The reduction in false positives indicates that the proposed detector algorithm better distinguished pressure and flow changes caused by normal operation from those caused by leakage.

The proposed detector proved effective under both Conditions I and II, with an overall detection delay of 0.38 ± 0.08 s, indicating consistent timing across trials with different defect sizes and locations. In Condition II, no false-positive alarms were attributed to bends or wall contact during navigation in the S-shaped phantom. This suggests that navigation-related pressure and flow variations did not produce residuals exceeding the alarm threshold for the required dwell time under the tested conditions. The single false negative in Table IV occurred after a prior false positive in the same trial. In the observed false-positive case, the measured inlet pressure temporarily fell below the commanded pressure, causing the regulator to supply additional inlet flow during pressure recovery even though no new control command was issued. This transient flow increase produced a positive residual for the required dwell time, although no leak had yet occurred.

Experiment 3 shows that automatic leak detection can reduce pressure exposure in a collapsed soft phantom by stopping pneumatic supply shortly after leak onset. This result supports the use of EKF-based detection as a safety layer during navigation, where continued pressurisation after leakage could otherwise increase environmental pressure. It must noted that the phantom pressure P_{env} represents a global measurement inside the test environment rather than the local stress on the phantom. For clinical implementation, the automatic cutoff should be accompanied by a clear visual or audible alert, allowing the operator to inspect the system before manually authorizing a restart.

TABLE V: Experiment 3: Leak mitigation performance (mean $\pm$ SD, $n = 10$ trials per mode).

Metric	Detection OFF	Detection ON (EKF)
$P_{\max}$ (bar)	0.12 ± 0.05	0.049 ± 0.01
$\bar{P}_{\mathrm{env}}$ (bar)	0.07 ± 0.006	0.008 ± 0.003
Detection delay (s)	N/A (detector disabled)	0.41 ± 0.13
False negatives	N/A (detector disabled)	0/10
False positives	N/A (detector disabled)	0/10

This study has several limitations. Defect size, location, and environment were varied together, preventing assessment of their individual effects. The minimum detectable leak size remains unknown, as small or intermittent leaks may generate insufficient residuals. Only punctures were tested, while slits and irregular tears may behave differently during eversion and wall contact. The algorithm also does not estimate defect size or leakage rate. Phantom-based validation also limits clinical generalisability. Peristaltic contractions may alter pressure and flow, causing false alarms or delayed detection. The phantom did not fully reproduce bowel geometry, tissue compliance, or gas escape conditions affecting pressure accumulation. Although supply cutoff reduced phantom pressure, its ability to prevent bowel injury requires further investigation.

Future studies will extend the proposed algorithm beyond binary leak detection to estimating leak magnitude. Controlled experiments with independently varied defect sizes and locations will establish detection limits, while testing across different operating conditions will assess robustness. Finally, ex vivo experiments on bowel tissue will evaluate whether automatic supply cutoff can limit tissue loading and injury following leakage.

REFERENCES

[1] I. Levy *et al.*, "Complications of diagnostic colonoscopy, upper endoscopy, and enteroscopy," *Best Pract. Res., Clin. Gastroenterol.*, 2016.
[2] J. F. Ahmed *et al.*, "Reducing applied force in colonoscopy using a novel soft robotic colonoscope: a head-to-head study," *Endosc. Int. Open*.
[3] E. W. Hawkes *et al.*, "A soft robot that navigates its environment through growth," *Sci. Robot.*, vol. 2, no. 8, p. 3028, July 2017.
[4] K. Borvorntanajanya *et al.*, "Model-based tracking control of a soft growing robot for colonoscopy," *IEEE Trans. Med. Robot. Bionics*, vol. 6, no. 4, pp. 1354–1362, 2024.
[5] Berthet-Rayne *et al.*, "Mammobot: A miniature steerable soft growing robot for early breast cancer detection," *IEEE Robot. Autom. Lett.*, vol. 6, no. 3, pp. 5056–5063, July 2021.
[6] J. Shi *et al.*, "Design, control, and evaluation of a novel soft everting robot for colonoscopy," *IEEE Trans. Robot.*, vol. 41, 2025.
[7] K. Borvorntanajanya *et al.*, "A pneumatic force sensor for enhanced force feedback in robotic colonoscopy," *IEEE Transactions on Medical Robotics and Bionics*, vol. 7, no. 4, pp. 1377–1388, 2025.
[8] A. Dehal and D. J. Tessier, "Intraperitoneal and extraperitoneal colonic perforation following diagnostic colonoscopy," *J. Soc. Laparoendosc. Surg.*, vol. 18, pp. 136–141, 2014.
[9] R. Kozarek *et al.*, "Air-pressure-induced colon injury during diagnostic colonoscopy," *Gastroenterology*, vol. 78, no. 1, pp. 7–14, 1980.
[10] S. Terryn *et al.*, "Self-healing soft pneumatic robots," *Science Robotics*, vol. 2, no. 9, 2017.
[11] K. Tabrizian *et al.*, "Toward autonomous self-healing in soft robotics: A review and perspective for future research," *Advanced Intelligent Systems*, vol. 7, no. 8, p. 2400790, 2025.
[12] J. P. Wilson, C. M. Best, and M. D. Killpack, "Variable stiffness adaptation to mitigate system failure in inflatable robots," in *ICRA*, 2017.
[13] M. Pontin and D. D. Damian, "Multimodal soft valve enables physical responsiveness for preemptive resilience of soft robots," *Science Robotics*, vol. 9, no. 92, 2024.
[14] S. Hoang *et al.*, "Error detection using pneumatic logic," *Device*, 2024.
[15] S. Zou *et al.*, "A retrofit sensing strategy for soft fluidic robots," *Nature Communications*, vol. 15, no. 539, 2024.
[16] T. George Thuruthel *et al.*, "Soft self-healing fluidic tactile sensors with damage detection and localization abilities," *Sensors*, 2021.
[17] K. Borvorntanajanya *et al.*, "Development of a low pressure pouch sensor for force measurement in colonoscopy procedures," in *IROS*, 2024.
[18] D. Kim *et al.*, "Probabilistic modeling and bayesian filtering for improved state estimation for soft robots," *IEEE Trans. Robot.*, 2021.

Authorized licensed use limited to: Imperial College London. Downloaded on November 21,2026 at 20:48:29 UTC from IEEE Xplore. Restrictions apply.
© 2026 IEEE. All rights reserved, including rights for text and data mining and training of artificial intelligence and similar technologies. Personal use is permitted, but republication/redistribution requires IEEE permission. See https://www.ieee.org/publications/rights/index.html for more information.